CISM International Centre for Mechanical Sciences 599
Courses and Lectures

Laura De Lorenzis
Alexander Düster *Editors*

Modeling in Engineering Using Innovative Numerical Methods for Solids and Fluids

International Centre for Mechanical Sciences

Springer

CISM International Centre for Mechanical Sciences

Courses and Lectures

Volume 599

For more than 40 years the book series edited by CISM, “International Centre for Mechanical Sciences: Courses and Lectures”, has presented groundbreaking developments in mechanics and computational engineering methods. It covers such fields as solid and fluid mechanics, mechanics of materials, micro- and nanomechanics, biomechanics, and mechatronics. The papers are written by international authorities in the field. The books are at graduate level but may include some introductory material.

More information about this series at http://www.springer.com/series/76

Laura De Lorenzis · Alexander Düster
Editors

Modeling in Engineering Using Innovative Numerical Methods for Solids and Fluids

Springer

Editors
Laura De Lorenzis
Institute of Applied Mechanics
Braunschweig University of Technology
Braunschweig, Germany

Alexander Düster
Numerical Structural Analysis with
Application in Ship Technology (M-10)
Hamburg University of Technology
Hamburg, Germany

ISSN 0254-1971 ISSN 2309-3706 (electronic)
CISM International Centre for Mechanical Sciences
ISBN 978-3-030-37517-1 ISBN 978-3-030-37518-8 (eBook)
https://doi.org/10.1007/978-3-030-37518-8

This Springer imprint is published by the registered company Springer Nature Switzerland AG
The registered company address is: Gewerbestrasse 11, 6330 Cham, Switzerland

Preface

Due to the ever-increasing computational power of modern computers, numerical simulations are of growing interest in many different fields of science and engineering. The fast-growing computer performance itself, however, is not sufficient to satisfy the increasing requirements for the simulation of complex problems arising in particular in fluid and solid mechanics. To this end, accurate and robust numerical methods are of crucial importance. The development of reliable and efficient discretization methods for solids and fluids supports the understanding of complex physical phenomena and helps to accelerate and improve the development of products and processes in almost all disciplines. Based on numerical simulation, the number of time-consuming and expensive experiments can be significantly reduced, and engineering decisions are supported by computed data which might be very difficult if not impossible to obtain experimentally.

This book stems from the lecture notes of the CISM course: *Modeling in Engineering Using Innovative Numerical Methods for Solids and Fluids* which was held in Udine on October 15–19, 2018. Innovative and promising modeling and simulation approaches are presented, including the basics of the methods as well as advanced topics and complex applications. The contents cover the following topics:

- Particle methods addressing particle-based materials and numerical methods that are based on discrete element formulations.
- Fictitious domain methods, which allow for the efficient discretization of complex problems for which meshing with finite elements is very difficult.
- Phase field models, which have become very popular to model and simulate fracture problems (among other possible applications).
- Computational fluid dynamics based on modern finite volume schemes to efficiently discretize the Navier–Stokes equations.
- Hybridizable discontinuous Galerkin methods, which offer high convergence rates for the simulation of incompressible flow problems.
- Non-intrusive coupling methods for structural models that allow to perform model adaptive simulations based on existing well-developed solvers.

The book is addressed to scientists and engineers from both academia and industry working in the broad field of civil and mechanical engineering or applied physics and mathematics. The intention is to provide a sound introduction to innovative numerical methods for solids and fluids which can be used to model complex problems in engineering.

Braunschweig, Germany — Laura De Lorenzis
Hamburg, Germany — Alexander Düster

Contents

Discrete Element Methods: Basics and Applications in Engineering

Peter Wriggers and B. Avci

Introduction

Particle systems are of great importance in many industrial branches like in chemical and food industries as well as in geotechnical engineering problems. Coupling of particles with fluids are related to fluvial erosion, fluidized beds, sedimentation and transport in the blood system. Thus, the numerical simulation of particle systems is of great interest, both from practical and fundamental points of view. Therefore, the understanding, the simulation and analysis of related phenomena is significant, particularly with regard to micro movements, homogenization procedures and coupled moderate or highly concentrated particulate flows. Certainly, such problems require an accurate description of the underlying physics, but the simulation of particulate flow and movement is still a challenging task for a large number of particles.

Popular examples of pure particle methods are Molecular Dynamics (MD), see Alder and Wainwright (1957), Discrete Element Method (DEM), see Cundall and Strack (1979), and Smoothed Particle Hydrodynamics (SPH), see Gingold and Monaghan (1977). In these methods, the positions of the particles and the evolution of their quantities are described by ordinary differential equations and solved in a Lagrangian way. In the framework of DEM and SPH, the particle dynamics are obtained by applying the Newton-Euler equations and the Navier-Stokes equations, respectively. Both of these numerical techniques (DEM and SPH) utilize many common algorithms, such as neighbor search algorithms, distance compu-

P. Wriggers (✉)
Faculty of Mechanical Engineering, Institut for Continuum Mechanics,
Leibniz University Hannover, Hannover, Germany
e-mail: wriggers@ikm.uni-hannover.de

B. Avci
CADFEM GmbH, Hannover, Germany

L. De Lorenzis and A. Düster (eds.), *Modeling in Engineering Using Innovative Numerical Methods for Solids and Fluids*, CISM International Centre for Mechanical Sciences 599,
https://doi.org/10.1007/978-3-030-37518-8_1

tations among neighboring particles and force or kernel evaluations. Thus, many subroutines can be implemented, used and maintained in a single framework.

In the recent years, effort has been made to improve the existing methods and to develop new efficient numerical approaches. Among the various methods evolved so far, e.g., see Zhu et al. (2007), Zohdi (2007), Pöschel and Schwager (2005) for an overview, the approaches for the treatment of particle systems through direct numerical simulation models are of high computationally cost. Basically, direct numerical simulations can be performed by different discretization methods.

Concerning the treatment of the particle collision, the methods employed in the DEM can be classified into two main classes, which are characterized by hard particle contact (Alder and Wainwright 1957) and soft particle contact (Cundall and Strack 1979). Methods assigned to the first of the two groups are instantaneous collision models. Here, the particles separate immediately from each other in the event of collision. They undergo no deformation, so they are considered to be rigid. In the other approach the particles are treated as quasi rigid objects such that they are assumed to suffer minute deformations during the collision. The force based methods of the second group can be applied to govern the contact forces implying the particles' strength and eventually also allow to locally break a particle if very strong forces act on it. The difference of the methods for the treatment of particle contact is particularly crucial in highly concentrated systems. Here, a particle will usually collided with more than one partner at the same time. Hence some particles might be as well in a permanent contact situation with neighboring particles like it occurs in a heap of sediments or in case of agglomerated adhesive particles. In these cases, the application of hard contact models may not be suitable. In contrast, force based soft contact models are applicable both for dense and dilute systems. However, the computation of particle interactions is for soft spheres much more expensive compared to the hard particle approach since very small time steps are needed to resolve the contact interaction between the particles in time.

Other applications—like sediment transport or multiscale computation for granular materials—are related to coupling discrete elements to solids and fluids. In case of a direct numerical simulation of 3D particulate flows one has to couple fluids and particles. This can be done in different ways that span the bridge from just tracing of particles to a full interaction of particle and fluid via the tractions. The latter can be based on a complex ALE finite element scheme using a adaptive remesching of the finite elements to follow the particle movement, see e.g. Johnson and Tezduyar (1997), but is—due to the high computational effort—often limited to a small amount of particles. Another approach is the fictitious domain method which can handle much more particles in the flow. In both approaches the numerical tools of DEM and FEM are appropriately coupled by a staggered scheme. To describe the collision between particles, the soft contact approach is applied using repulsive force models. For more details see e.g. Avci and Wriggers (2012).

When coupling finite elements for solids and discrete elements there are two different possibilities. The first is a surface coupling where contact between a finite and a discrete element takes place. This can be handled by standard contact algorithms, see e.g. Wriggers (2006). On the other hand it is possible to couple finite and dis-

crete elements within a volume. Such coupling requires specific treatment of linking the movement of the finite and the discrete elements. On possibility is the Arlequin methodology, see e.g. Dhia and Rateau (2005), which was applied with respect to particle and finite element coupling in Wellmann and Wriggers (2012).

Governing Equations

The motion of a quasi rigid particle $\mathcal{P}_i$ is described by a position vector $\mathbf{X}_i$ to its center of mass and a rotation Ψ_i at time $t = t_0$. In Fig. 1 the kinematics of the movement of the particle $\mathcal{P}_i$ is depicted for different time instants. Additionally another particle $\mathcal{P}_j$ is depicted that collides with particle $\mathcal{P}_i$.

The trajectory of particle $\mathcal{P}_i$ can be deduced from the Newton-Euler equations. Consequently its translational and angular velocities, $\mathbf{u}_i = \dot{\mathbf{x}}_i$ and $\boldsymbol{\omega}_i = \frac{\mathrm{d}\Psi_i}{\mathrm{d}t}$, have to satisfy

$$M_i \frac{\mathrm{d}^2 \mathbf{x}_i}{\mathrm{d}t^2} = \rho_i \, V_i \mathbf{g} + \mathbf{F}_i \tag{1}$$

$$\Theta_i \frac{\mathrm{d}\boldsymbol{\omega}_i}{\mathrm{d}t} + \boldsymbol{\omega}_i \times (\Theta_i \boldsymbol{\omega}_i) = \mathbf{T}_i \, . \tag{2}$$

Therein, M_i is the mass, $\mathbf{x}_i$ the position vector at time t to the center of mass (defined as $\mathcal{M}_i$), ρ_i the mass density, $\mathbf{g}$ the gravity and V_i denotes the volume of the particle $\mathcal{P}_i$. The tensor of inertia is represented by Θ_i. Furthermore, the sum of the contact forces is stated as $\mathbf{F}_i$ The torques that are caused by $\mathbf{F}_i$ with respect to $\mathcal{M}_i$ are associated to the quantities $\mathbf{T}_i$. The traction vector $\mathbf{t}$ on $\partial\boldsymbol{\Omega}_p$ is defined by $\mathbf{t} = \sigma \mathbf{n}_f$ where $\mathbf{n}_f$ is the unit outward normal vector and $\mathbf{r}_i$ is the position vector of a point at $\partial\boldsymbol{\Omega}_p$ with respect to $\mathcal{M}_i$.

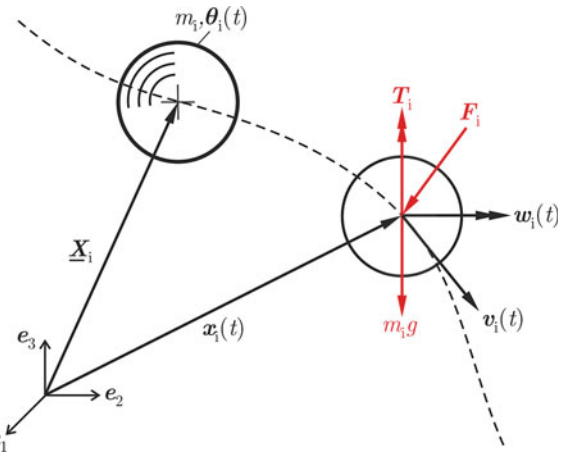

Fig. 1 Kinematics and applied forces related to a particles

Constitutive Modeling of the Particle Phase

The particles are modeled as quasi rigid spheres. To describe their collision behavior, a force based approach is used in order to govern the inter-particle forces that are deduced from repulsive models. In the sections below, the relevant concepts of the contact models are stated.

Normal Contact Model

The normal contact force acting between the colliding particles is described by a constitutive viscoelastic model. For adhesive particles being in contact, the attractive van der Waals force is additionally considered in the contact area. For the purpose of governing the elastic contact force F_e^n, the Hertzian law (Hertz 1882) constitutes a well-established model. If the particles, to be treated, have also viscous material properties a consistent phenomenological model has to be employed, see e.g., Refs. (Brilliantov et al. 1996, 2007), where the effect of viscosity is considered via an added dissipative force F_d^n. Regarding the presence of the attractive van der Waals force in the contact area, the JKR theory, see Johnson et al. (1971), provides a proper treatment of adhesion, even in the case of underwater adhesion, see e.g. Loskofsky et al. (2006). For a detailed description of the JKR model see also Maugis (1992).

If adhesion is considered, the attractive force F_a^n acts against the elastic force F_e^n so that it consequently reduces the particles' compression. Thus, one obtains for the force acting on a particle

$$F^n = F_e^n - F_a^n + F_d^n \,. \tag{3}$$

Hertz Law

When using the Hertzian contact law Hertz (1882), the elastic repulsive force is governed by

$$F_e^n = \frac{4}{3} E \sqrt{R}\, \delta^{3/2} \,, \tag{4}$$

where $\delta = \delta_i + \delta_j$ is the total particle compression which is also called the approach of the particles. The values

$$R = \left(\frac{1}{R_i} + \frac{1}{R_j} \right)^{-1} \quad \text{and} \quad E = \left(\frac{1 - \nu_i^2}{E_i} + \frac{1 - \nu_j^2}{E_j} \right)^{-1} \tag{5}$$

denote the effective radius and the effective Young's modulus of the contact pair $\mathcal{P}_i$ and $\mathcal{P}_j$, respectively. The Poisson ratio is associated with the particles as ν_i and ν_j.

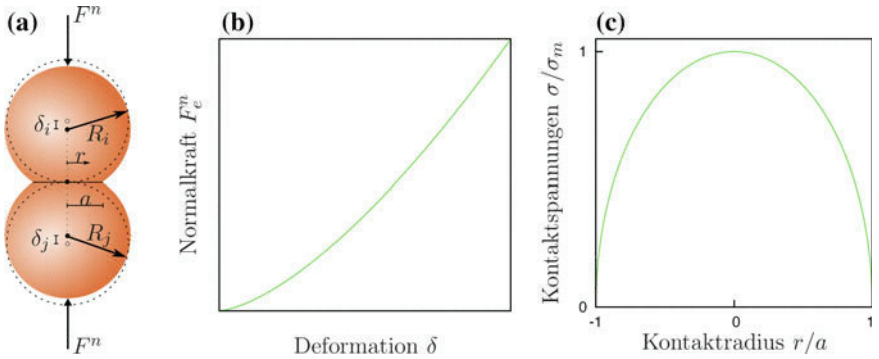

Fig. 2 Hertz contact law

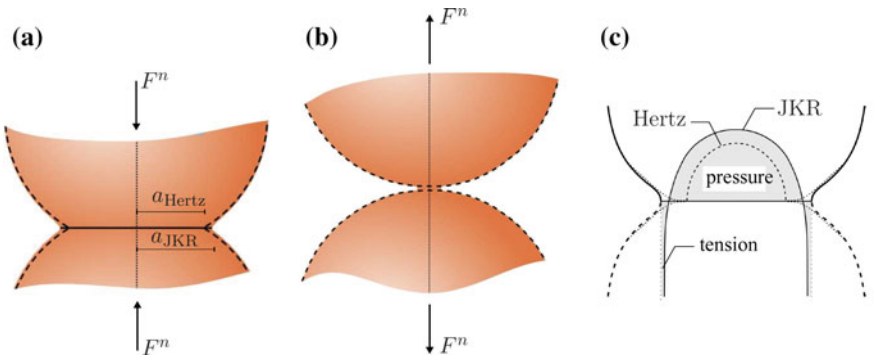

Fig. 3 Adhesion in the contact interface

As a result of the mutual compression of the particles, a circular area is formed in the contact zone. One can deduct that 1 the radius a of the shaped contact area is related to the total deformation δ via $a^2 = R\delta$.

Figure 2 depicts the deformation state that is assumed locally within the quasi rigid spheres. It also shows the relation between approach δ of the two spheres with respect to the force F^n. One can easily see the nonlinearity of the Hertz law. Furthermore the distribution of the contact pressure σ/σ_m depending on the contact radius r/a is depicted in the right part of the figure. Here $\sigma = F^n/(\pi\, a^2)$ and $\sigma_m = \max \sigma$.

Adhesion Law

According to the JKR model, see Johnson et al. (1971), it is implied that the adhesive force acts only within the contact area, see Fig. 3. Here, the work of adhesion under a liquid or just the free energy changes to separate a unit contact area of $\mathcal{P}_i$ and $\mathcal{P}_j$ in a liquid medium (l) is defined as

$$W = \gamma_{il} + \gamma_{jl} - \gamma_{ij}, \tag{6}$$

where γ describes the respective interfacial energy, see Loskofsky et al. (2006). Since the adhesive force F_a^n is opposed to the elastic force F_e^n, it reduces the elastic deformation δ_e leading to

$$\delta_e - \delta_a = \frac{a^2}{R} - \sqrt{\frac{2\pi\, W a}{E}}, \tag{7}$$

where δ_e is obtained from the Hertzian law, the second term δ_a is due to adhesion, see Maugis (1992) for details. The corresponding forces follow as

$$F_e^n - F_a^n = \frac{4Ea^3}{3R} - 2\pi a^2 \sqrt{\frac{2WE}{\pi a}}. \tag{8}$$

In case of the absence of external forces, i.e. $F^n = 0$, then $F_a^n \neq 0$ while $F_e^n = 0$ and $F_e^d = 0$. Furthermore, an equilibrium contact area a_0 is formed in the contact zone where a mutual compression δ_0 of the particles occurs

$$a_0 = \left(\frac{9\pi\, WR^2}{2E}\right)^{1/3} \quad \text{and} \quad \delta_0 = \left(\frac{3R}{4}\left(\frac{\pi\, W}{E}\right)^2\right)^{1/3}. \tag{9}$$

To pull the particles off each other, one has to apply a traction force under which they suffer minute stretching deformations forming a connecting neck around the contact zone. Once the pulling force has reached a critical level, i.e. $F^n = -F_c^n$, the contact breaks and the particles will separate. The critical force F_c^n yields

$$F_c^n = \frac{3}{2}\pi\, WR \tag{10}$$

and the corresponding critical distance of the particles follows

$$\delta_c = \frac{1}{48^{1/3}} \frac{a_0^2}{R}. \tag{11}$$

Here the pulling distance can be defined as $\delta = -\delta_c$. Figure 4 demonstrates the differences in the force.

Viscous Effects in the Contact Interface Law

Viscous properties can be modeled using the system depicted in Fig. 5 for two spheres (a) and one sphere (b) being in contact wth a rigid wall. The forces in the damper d are provided below.

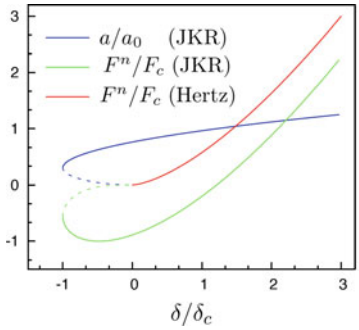

	δ/δ_c	a/a_0	F^n/F_c
Contact	0	$(2/3)^{2/3}$	$-8/9$
Equilibrium	$(4/3)^{2/3}$	1	0
Lift-Off	-1	$(1/6)^{2/3}$	$-5/9$

Fig. 4 Forces in the contact interface due to Hertz and the JKR model

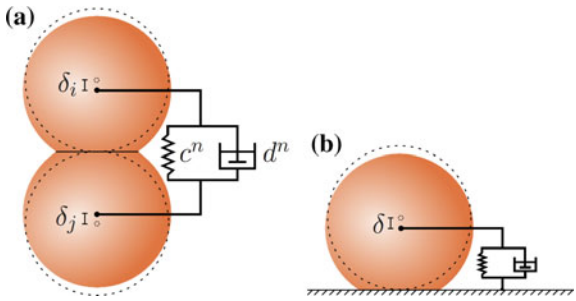

Fig. 5 Viscous effects in the contact interface

To consider the properties of material viscosity, a dissipative force is adopted according to the work of Brilliantov et al. (1996, 2007) which yields

$$F_d^n = A\dot{a}\frac{\partial}{\partial a}(F_e^n - F_a^n)\,. \tag{12}$$

From this definition, the viscous force follows as

$$F_d^n = \dot{a}A\left(\frac{4Ea^2}{R} - \frac{3}{2}\sqrt{8\pi\, WEa}\right), \tag{13}$$

where the dissipative factor[1] A is related to a constant function of material viscosity. Consequently, considering the above set of equations, one obtains the force-displacement relation for adhesive viscoelastic particles

[1]This factor A can also be used as a fitting parameter within specific simulations—like quasistatic predictions of granular material behaviour—to damp oscillations.

$$F^n(\delta) = \frac{4}{3} E \sqrt{R} \delta^{3/2} - 2R^{3/4} \delta^{3/4} \sqrt{2\pi\, W E} + A\dot{\delta} \left(2E\sqrt{R}\sqrt{\delta} - 3\sqrt{\frac{1}{2} R^{3/2} \pi\, W E \delta^{1/4}} \right). \tag{14}$$

Computation of the Approach

In the present contribution, the constitutive law given in (4) and (14) is treated analogous to the penalty method, e.g., see Wriggers (2006) and Wellmann et al. (2008). In this methodology one computes the force F_e^n between to particles $\mathcal{P}_i$ and $\mathcal{P}_j$ is computed from the approach of two particles by using the interface law (in case of the classical penalty approach this equation is $F_e^n = \varepsilon_P\, \delta$ with the spring stiffness, know as penalty parameter, ε_P). However in this case the penalty spring is nonlinear, see e.g. Eq. (4).

In all constitutive equations above the approach of the spheres or the rate of this approach has to be evaluated. For this one can compute the gap in normal direction g_n from the given current positions of two spheres

$$g^n = (R_i + R_j) - l > 0, \tag{15}$$

and define $g^n \equiv \delta$ as the mutual compression or approach of $\mathcal{P}_i$ and $\mathcal{P}_j$. With this kinematic relation the contact forces can be immediately computed by evaluating (4) and (14). In Eq. (15) $l = ||\mathbf{l}||$ is the length of the distance vector between $\mathcal{M}_i$ and $\mathcal{M}_j$ in the current configuration, where $\mathbf{l} = \mathbf{x}_i - \mathbf{x}_j$. The deformation rate $\dot{\delta}$ is computed in Eq. (16) by the projection of the relative velocity $(\mathbf{v}_i - \mathbf{v}_j)$ onto the direction of the normal unit vector $\mathbf{n}$. This yields

$$\dot{\delta} = \dot{g}^n = -(\mathbf{v}_i - \mathbf{v}_j) \cdot \mathbf{n} \quad \text{where} \quad n = l/l. \tag{16}$$

We note that the direction of the contact force F^n of the respective particle is opposite to the direction of compression δ. Based on this observation, one can deduct from (14) the contact force $\mathbf{F}^n = F^n \mathbf{n}$ that contributes to the momentum equation (1).

Tangential Contact Model

The constitutive relation of Coulomb's law couples the tangential force F^t to the normal force F^n. For this the coefficient of friction has to be introduced as a constitutive parameter. The relation is not smooth since for sliding

$$F^t = \mu_G F^n \tag{17}$$

holds while

$$F^t \leq \mu_H F^n \tag{18}$$

is valid for sticking. In this relation the dynamic and the static coefficients of friction have to be introduced. The parameter μ_G stands for sliding and μ_H for stick, where $\mu_G \leq \mu_H$. The relations between normal and tangential force are depicted in Fig. 6. Here (a) shows a simplified model of the real behaviour in (b) with $\mu_G = \mu_H$. Another simplified model is depicted in Fig. 6c which differentiates between the coefficient of friction for sticking and sliding.

Within the constitutive treatment for the tangential interface force F^t, a tangential spring-dashpot element with an incorporated slider is used in order to model the tangential friction behaviour, see e.g. Cundall and Strack (1979). This model is depicted in Fig. 7 where again the difference between the tangential contact of two particles and of a particle with a rigid wall is made.

Since the tangential part of the interface force F^t is related to two states, sliding and sticking, it can be viewed like an elasto-plastic process where sliding relates to the plastic flow. For these types of problems efficient algorithms were developed in the mid 1980s. The first application to frictional contact can be found in Wriggers (1987) and has been further developed over the years, see e.g. Wriggers et al. (1990), Luding (2004) and Wriggers (2006). The idea is to algorithmically predict first a "trial" stick step followed by a slip check in the second step. Then the regularized penalty formulation for the tangential trial traction takes the form

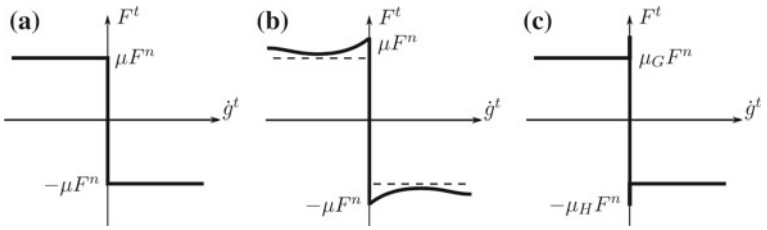

Fig. 6 Friction states with stick and sliding

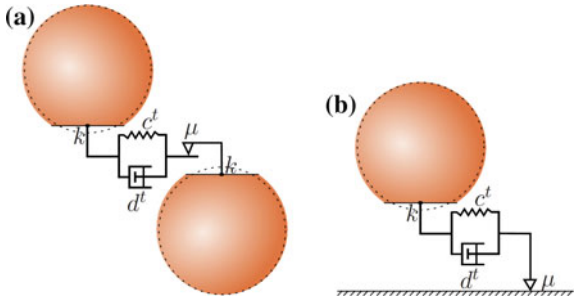

Fig. 7 Friction states with stick and sliding

$$\mathbf{F}_o^t = -(c^t \mathbf{g}^t + d^t \mathbf{v}^t). \tag{19}$$

Therein, $\mathbf{g}^t$ is the elongation of the tangential spring, c^t and d^t are the tangential spring stiffness and the tangential dissipation parameter, respectively. The tangential relative velocity at the contact point $\mathcal{C}$ is given by

$$\mathbf{v}^t = \mathbf{v}^s - (\mathbf{v}^s \cdot \mathbf{n})\,\mathbf{n} \tag{20}$$

with the relative velocity at $\mathcal{C}$

$$\mathbf{v}^s = \mathbf{v}_i^{\mathcal{C}} - \mathbf{v}_j^{\mathcal{C}}, \tag{21}$$

where the surface velocities are defined by $\mathbf{v}_i^{\mathcal{C}} = \mathbf{U}_i + \boldsymbol{\omega}_i \times \mathbf{r}_i$ and $\mathbf{v}_j^{\mathcal{C}} = \mathbf{U}_j + \boldsymbol{\omega}_j \times \mathbf{r}_j$. The vectors pointing from $\mathcal{M}_i$ and $\mathcal{M}_j$ to $\mathcal{C}$ are associated with $\mathbf{r}_i = R_i(-\mathbf{n})$ and $\mathbf{r}_j = R_j\mathbf{n}$, respectively. By introducing a trial function f^{tr}, the following relation can be stated for the tangential contact

$$f^{\mathrm{tr}} =: ||\mathbf{F}_o^t|| - \mu_s ||\mathbf{F}^n|| \Rightarrow \begin{cases} \leq 0 & : \text{ Stick} \\ > 0 & : \text{ Slip.} \end{cases} \tag{22}$$

If $f^{\mathrm{tr}} \leq 0$ the contact point $\mathcal{C}$ is in the stick region and if $f^{\mathrm{tr}} > 0$ it is in slip region, thus sliding occurs in the contact area. Note that the stick case is valid again if $F_o^t < \mu_d F^n$ holds during the sliding process. If the contact point sticks, the actual tangential spring $\mathbf{g}^t$ is incremented for the succeeding time step by the relation $\Delta\mathbf{g}^t = \mathbf{v}^t \Delta t_{\mathrm{D}}$. Consequently, the new spring length is defined by

$$\overline{\mathbf{g}}^t = \mathbf{g}^t + \Delta\mathbf{g}^t\,. \tag{23}$$

Here, Δt_{D} denotes the time step of the discrete element method. However, if the contact point slides in the current time step, the tangential spring is aligned by

$$\overline{\mathbf{g}}^t = -\frac{1}{c_t}(F^t \mathbf{t} + d^t \mathbf{v}^t) \tag{24}$$

in order to fulfill Coulomb's slip condition. Therein, $\mathbf{t} = \mathbf{F}_o^t / ||\mathbf{F}_o^t||$ is the direction of the trial traction.

In two subsequent time steps, the contact area might be slightly rotated. As proposed in Luding (2004), the tangential spring is continuously projected onto the current rotated contact area at the beginning of each new time step via $\mathbf{g}^t = \overline{\mathbf{g}}^t - (\overline{\mathbf{g}}^t \cdot \mathbf{n})\mathbf{n}$. For the above approach, the tangential contact force is $F^t = ||\mathbf{F}_o^t||$ if $f^{\mathrm{tr}} \leq 0$ and $F^t = \mu_d F^n$ if $f^{\mathrm{tr}} > 0$ holds. By computing F^t, one obtains $\mathbf{F}^t = F^t\mathbf{t}$ and $\mathbf{T}^t = \mathbf{r} \times \mathbf{F}^t$ which contributes to $\mathbf{F}$ and $\mathbf{T}$ in Eq. (1) and Eq. (2), respectively.

Rolling Resistance Model

During a rolling motion of two particles over each other, the leading part of the contact area is continuously compressed and the trailing part is decompressed with respect to the rolling direction, see Fig. 8.

In case of an attractive van der Waals force in the contact area, the particles suffer an opposing torque to rolling motion, whereby a rolling resistance is generated. For instance, regarding an agglomerated straight particle chain with a lack of rolling resistance, the chain cannot resist any external impact resulting in a tangential force. As a consequence, the particles will roll smoothly over each other, whereby the chain easily bends and it will finally take a compact shape. For a detailed discussion of the rolling resistance of adhesive particles, see Dominik and Tielens (1995).

For a constitutive treatment of the rolling resistance, a model consisting of a rolling spring-dashpot-slider element is adopted in this contribution, see Iwashita and Oda (1998) and Fig. 9.

At this, the opposing torque is given by

$$\mathbf{M}_o^r = -(c^\varphi \phi + d^\varphi \dot{\phi}) = -\frac{1}{R}(c^\phi \mathbf{g}^r + d^\varphi \mathbf{v}^r). \tag{25}$$

Therein, c^φ is the rolling stiffness, d^φ relates to the rolling viscosity coefficient, ϕ to the particle rotation, $\mathbf{g}^r$ to the rolling distance and $\mathbf{v}^r$ is the rolling velocity which, according to Kuhn and Bagi (2004), can be computed using

$$\mathbf{v}^r = -R\left[(\boldsymbol{\omega}_i - \boldsymbol{\omega}_j) \times \mathbf{n} + \frac{1}{2}\left(\frac{1}{R_j} - \frac{1}{R_i}\right)\mathbf{v}^t\right]. \tag{26}$$

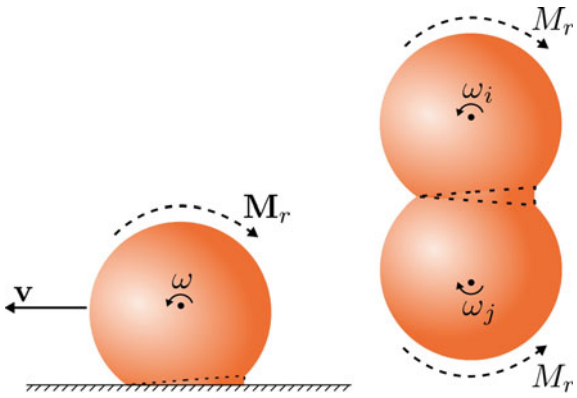

Fig. 8 Idea of rolling resistance

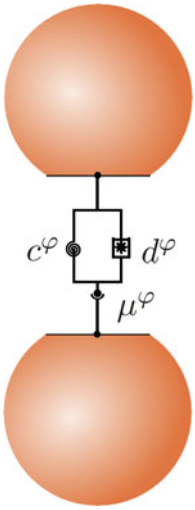

Fig. 9 Model of rolling resistance

In the context of the JKR theory one can set for c^ϕ the following expression

$$c^\varphi = 4F_c^n R\left(\frac{a}{a_0}\right)^{3/2} \qquad \text{where} \qquad d^\varphi = 0\,, \tag{27}$$

see Dominik and Tielens (1995) for details.

Introducing a trial force $\mathbf{F}_o^r = \mathbf{M}_o^r/R$, the problem of the rolling resistance can algorithmically be treated analogous to the tangential friction model. Here, one can apply as a yield criteria for the slider $M_{\max}^r$ or $\mu^r F^n$, where μ^r is a rolling friction coefficient, see Iwashita and Oda (1998).

DEM Solver

The kinematic variables of the particles are governed by the computation of the equations of motion (1) and (2). For this purpose, a time integration scheme has to be applied to solve these equations.

At the same time the contact between the particles has to be considered. This yields the different contact forces and moments between the particles. These forces and moments can be computed using the interaction laws discussed in the previous section.

Time Integration

Since DEM simulations usually need very small time steps Δt in order to resolve the constitutive laws between the particles the computational time for a larger system of particles is high. Thus time integration methods need to be considered very carefully. They have on one side to guarantee a certain accuracy and on the other side they need to be efficient and robust to solve the Newton-Euler-equations in (2). An overview with respect to methods that are used in DEM can be found in e.g. Kruggel-Emden et al. (2008).
The integration scheme is composed of three steps:

1. Predicting all the kinematic variables.
2. A force computation step is followed using the predicted variables according to Section "Constitutive Modeling of the Particle". Hence, the evolution of the translational and rotational accelerations can be computed from Eqs. (1) and (2).
3. Applying an error criteria between the predicted and calculated accelerations, the correction of the kinematic variables is ensued.

To illustrate the construction of such time integration scheme we consider a Gear algorithm in more detail. This starts with a predictor computation which is different for translation and rotation.
For the translation one computes

$$\begin{aligned}
\mathbf{x}^P(t+\Delta t) &= \mathbf{X}(t) + \dot{\mathbf{X}}(t)\Delta t + \frac{1}{2}\ddot{\mathbf{X}}(t)\Delta t^2 + \frac{1}{6}\dddot{\mathbf{X}}(t)\Delta t^3 \\
\dot{\mathbf{x}}^P(t+\Delta t) &= \dot{\mathbf{X}}(t) + \ddot{\mathbf{X}}(t)\Delta t + \frac{1}{2}\dddot{\mathbf{X}}(t)\Delta t^2 \\
\ddot{\mathbf{x}}^P(t+\Delta t) &= \ddot{\mathbf{X}}(t) + \dddot{\mathbf{X}}(t)\Delta t \\
\dddot{\mathbf{x}}^P(t+\Delta t) &= \dddot{\mathbf{X}}(t)
\end{aligned} \tag{28}$$

For the rotation the predictor is given by

$$\begin{aligned}
\boldsymbol{\omega}^P(t+\Delta t) &= \boldsymbol{\Omega}(t) + \dot{\boldsymbol{\Omega}}(t)\Delta t + \frac{1}{2}\ddot{\boldsymbol{\Omega}}(t)\Delta t^2 + \frac{1}{6}\dddot{\boldsymbol{\Omega}}(t)\Delta t^3 + \frac{1}{24}\overset{(iv)}{\boldsymbol{\Omega}}(t)\Delta t^4 \\
\dot{\boldsymbol{\omega}}^P(t+\Delta t) &= \dot{\boldsymbol{\Omega}}(t) + \ddot{\boldsymbol{\Omega}}(t)\Delta t + \frac{1}{2}\dddot{\boldsymbol{\Omega}}(t)\Delta t^2 + \frac{1}{6}\overset{(iv)}{\boldsymbol{\Omega}}(t)\Delta t^3 \\
\ddot{\boldsymbol{\omega}}^P(t+\Delta t) &= \ddot{\boldsymbol{\Omega}}(t) + \dddot{\boldsymbol{\Omega}}(t)\Delta t + \frac{1}{2}\overset{(iv)}{\boldsymbol{\Omega}}(t)\Delta t^2 \\
\dddot{\boldsymbol{\omega}}^P(t+\Delta t) &= \dddot{\boldsymbol{\Omega}}(t) + \overset{(iv)}{\boldsymbol{\Omega}}(t)\Delta t \\
\overset{(iv)}{\boldsymbol{\omega}}{}^P(t+\Delta t) &= \overset{(iv)}{\boldsymbol{\Omega}}(t)
\end{aligned} \tag{29}$$

Based on these predictions the force $\mathbf{F}^P(\mathbf{x}^P, \dot{\mathbf{x}}^P)$ and the moment $\mathbf{M}^P(\dot{\mathbf{x}}^P, \boldsymbol{\omega}^P)$ are computed which act both on a particle. Based on these quantities the translational and

rotational accelerations can be computed from (2). This yields $\mathbf{a}^* = \mathbf{F}^P/m$ and $\dot{\boldsymbol{\omega}}^* = \mathbf{M}^P/\Theta$. Now the differences $\Delta\ddot{\mathbf{x}} = \mathbf{a}^* - \ddot{\mathbf{x}}^P$ and $\Delta\dot{\boldsymbol{\omega}} = \dot{\boldsymbol{\omega}}^* - \dot{\boldsymbol{\omega}}^P$ can be determined for the corrector step in which the translations and rotations are corrected. For the translations it follows

$$\begin{aligned}
\mathbf{x}(t+\Delta t) &= \mathbf{x}^P(t+\Delta t) + c_0^t\,\mathbf{s}^t \\
\dot{\mathbf{x}}(t+\Delta t) &= \dot{\mathbf{x}}^P(t+\Delta t) + c_1^t\,\mathbf{s}^t\,\frac{1}{\Delta t} \\
\ddot{\mathbf{x}}(t+\Delta t) &= \ddot{\mathbf{x}}^P(t+\Delta t) + c_2^t\,\mathbf{s}^t\,\frac{2}{\Delta t^2} \\
\dddot{\mathbf{x}}(t+\Delta t) &= \dddot{\mathbf{x}}^P(t+\Delta t) + c_3^t\,\mathbf{s}^t\,\frac{6}{\Delta t^3}
\end{aligned} \tag{30}$$

and the rotations are obtained from

$$\begin{aligned}
\boldsymbol{\omega}(t+\Delta t) &= \boldsymbol{\omega}^P(t+\Delta t) + c_0^r\,\mathbf{s}^r \\
\dot{\boldsymbol{\omega}}(t+\Delta t) &= \dot{\omega}^P(t+\Delta t) + c_1^r\,\mathbf{s}^r\,\frac{1}{\Delta t} \\
\ddot{\boldsymbol{\omega}}(t+\Delta t) &= \ddot{\boldsymbol{\omega}}^P(t+\Delta t) + c_2^r\,\mathbf{s}^r\,\frac{2}{\Delta t^2} \\
\dddot{\boldsymbol{\omega}}(t+\Delta t) &= \dddot{\boldsymbol{\omega}}^P(t+\Delta t) + c_3^r\,\mathbf{s}^r\,\frac{6}{\Delta t^3} \\
\overset{(iv)}{\boldsymbol{\omega}}(t+\Delta t) &= \overset{(iv)}{\boldsymbol{\omega}}{}^P(t+\Delta t) + c_4^r\,\mathbf{s}^r\,\frac{24}{\Delta t^4}
\end{aligned} \tag{31}$$

with the constants

$$\mathbf{s}^t = \frac{\Delta t^2}{2}\Delta\ddot{\mathbf{x}}\,,\; c_0^t = \frac{1}{6}\,,\; c_1^t = \frac{5}{6}\,,\; c_2^t = 1\,,\; c_3^t = \frac{1}{3}$$

and

$$\mathbf{s}^r = \Delta t\,\Delta\dot{\boldsymbol{\omega}}\,,\; c_0^r = \frac{251}{720}\,,\; c_1^r = 1\,,\; c_2^r = \frac{11}{12}\,,\; c_3^r = \frac{1}{3}\,,\; c_4^r = \frac{1}{24}$$

Within this method of Gear the translations are approximated by a Taylor expansion of 3rd order while the rotations have to be modeled by a 4th order Taylor expansion. This choice is necessary to achieve conservation of momentum and moment of momentum and a good accuracy of the solution. A more complete description of the Gear algorithm can be found in Allen and Tildesley (1987), Pöschel and Schwager (2005).